technologies

MDPI

Article

Interactions between the Ionic Liquid and the ZrO_2 Support in Supported Ionic Liquid Membranes for CO_2 Separation

Cinthia E. Sánchez-Fuentes [1], Sibele B. Pergher [2], Mirella Gutiérrez-Arzaluz [3], Violeta Mugica-Álvarez [1], Eduardo Terrés [4] and Miguel Torres-Rodríguez [3,*]

1 Posgrado en Ciencias e Ingeniería de Materiales, Universidad Autónoma Metropolitana Azcapotzalco, Ciudad de México 02200, Mexico; sirenka86_@hotmail.com (C.E.S.-F.); vma@correo.azc.uam.mx (V.M.-Á.)
2 Laboratório de Peneiras Moleculares, PPGQ, Instituto de Química, Universidade Federal do Rio Grande do Norte, Natal RN 59078-970, Brasil; sibelepergher@gmail.com
3 Departamento de Ciencias Básicas, Universidad Autónoma Metropolitana Azcapotzalco, Ciudad de México 02200, Mexico; gam@correo.azc.uam.mx
4 Instituto Mexicano del Petróleo, Ciudad de México 07730, Mexico; eterres@imp.mx
* Correspondence: trm@correo.azc.uam.mx; Tel.: +52-55-5318-9570

Academic Editor: Gustavo A. Fimbres Weihs
Received: 16 June 2016; Accepted: 15 September 2016; Published: 28 September 2016

Abstract: This work reports the interaction study of two supported ionic liquid membranes (SILMs) based on 1-butyl-3-methylimidazolium hexafluorophosphate ($[C_4mim][PF_6]$) and 1-butyl-3-methylimidazolium tetrafluoroborate ($[C_4mim][BF_4]$), which were impregnated into porous zirconia supports with 20 nm average pore diameters. The interaction of ionic liquid-support observed from diffuse reflectance (DR), Fourier transform infrared spectroscopy (FTIR) and scanning electron microscopy and energy dispersive spectroscopy (SEM/EDS) is reported. The IR spectrum in the 600 to 4000 cm^{-1} range showed a specific interaction of the ionic liquid with the support. The N_2 and CO_2 permeances in the SILMs with $[C_4mim][BF_4]$ were 8.7×10^{-8} $mol \cdot s^{-1} \cdot m^{-2} \cdot Pa^{-1}$ and 9.6×10^{-7} $mol \cdot s^{-1} \cdot m^{-2} \cdot Pa^{-1}$, respectively. The separation factor through the ionic liquid in the membrane as a function of temperature showed that the SILMs studied here can be used for CO_2 separation at low temperatures.

Keywords: CO_2; ionic liquid; SILMs; FTIR; permeance; separation factor

1. Introduction

Some properties of ionic liquids (ILs), such as negligible vapour pressures and high viscosities, make them adequate candidates for the liquid phase in supported ionic liquid membranes (SILMs). Additionally, a slow outward liquid displacement happens from a micro or mesoporous support under pressure, which reduces the loss of ILs from the supports [1]. The current materials that can support ionic liquids for gas separation in post-combustion processes, in which the goal is to separate CO_2 from CO_2/N_2 mixtures, can be categorized into inorganic ceramic and organic polymeric materials. When comparing the two types of membranes, it has been shown that ceramic membranes exhibit quite good performances, permeances, and selectivity separation factors, and can be operated up to 350 °C. In contrast, the working temperature of polymeric membranes is below 200 °C [2]. The CO_2 separation membrane can be either a single or composite structure made of, for example, silica, zeolite, zirconia, titania, or alumina [3,4]. Among these, zirconia is an especially attractive material for ceramic membranes. A zirconia-based membrane exhibits excellent features, including elevated chemical stability, superior permeability, and greater flux during separation owing to its specific surface characteristics and excellent thermal resistance [5].

Recently, Tomé and Marrucho [6] have endeavoured to describe, in detail, various classical separation techniques, absorption, adsorption, cryogenic distillation, and with membranes, and also included techniques for CO_2 separation using ILs, paying special attention to operating conditions and different types of ILs, also for the separation of biomethane CO_2/CH_4, post-combustion processes CO_2/N_2, and pre-combustion CO_2/H_2 flue gas. Particular attention was devoted to reviewing the progress of materials based on ionic liquids and the possibility to synthesize them with specific properties for the separation of CO_2 in different gas mixtures streams. Therefore, intense efforts have been devoted recently to the development of syntheses of ionic liquids with specific control over chemical functions of the anion and cation, functionalized ILs-based, new generations of polymer/ILs-based gel membrane and, lately, poly (ionic liquid) membranes; all of these materials are oriented to a more CO_2-efficient separation in terms of chemical functionalities, specific to the separation from flue gas streams. Today there exist challenges that ILs-based membranes need resolving for their use in CO_2 separation from flue gases, that are simultaneously thermally-, plasticization- and aging-resistant, etc.

This year Dai et al. [7] reviewed an important number of studies on SILMs that used conventional ILs based on physical absorption; of note, gas transport in this condition in SILMs is based on a solution-diffusion mechanism, although their selectivities are driven by differences in the physical solubility of gases in the ILs. The reviewed highlights described the use of porous ceramic supports; the authors underlined the achievement of greater thermal and mechanical stability of the SILMs, which was attributed to the pore size of the support. The ILs-based membrane's contactor offer a well-defined interfacial area and stable, independent control of the gas rate, and liner up-scaling, among other advantages for CO_2 capture at low pressure and temperature. Despite the progress reported in recent years, there are still challenges that are important to solve for an industrial application; for instance, the ILs have relatively low surface tension, which facilitates the membrane's pore-wetting, toxicity levels, a potential environmental impact, and their relative high price. Finally, another important aspect stated the need to give attention to: " ... better understanding of structures-properties relationship of ILs and the desired properties suitable for ILs-based membranes" [7].

Moreover, Rodríguez et al. [8] showed that an imidazolium-based ionic liquid immobilized on a silica support exhibited strong interactions of both [C_4mim] and hexafluorophosphate ions with the silica surface. However, for a [C_4mim][PF_6]/Al_2O_3 composite, the temperature rise provoked a loss of the supramolecular arrangement, and a decrease in the thermostability of the ILs in [C_4mim][PF_6]/Al_2O_3 was observed. The foremost advantage in using ILs is that their properties (e.g., viscosity, Lewis acidity, hydrophobicity, gas solubility), can be tuned by using suitable cations and anions to obtain specific solvent properties. These features are what make ILs promising potential alternatives for gas separation. Good gas solubility is necessary for using ILs sin SILMs in gas separation, because SILMs permeability depends on gas solubility.

Furthermore, several groups have studied CO_2 solubility in various ionic liquids and determined a higher solubility relative to other gases, such as CH_4 and N_2. In this regard, Blath et al. showed a greater CO_2 solubility in ILs at 60 °C compared with other gases such as CH_4, N_2, and CO, indicating that it was the most promising gas for absorption in ILs, which would allow ILs to be used for separating mixtures containing CO_2 [9]. Therefore, several research investigations have successfully used ionic liquids with imidazolium as the cation and hexafluorophosphate and tetrafluoroborate as anions for gas separation. A study conducted by Kanakubo [10] showed that CO_2 molecules were favourably solvated to hexafluorophosphate anions, which suggests van der Waals interactions from the Lewis acid–base interactions between fluorine of the anion, the interactions between the fluorine groups of the anion, and the carbon in CO_2, as shown by Kerlé and Anthony et al. [11–13] through molecular dynamics simulations.

In addition, a key factor to consider is the contact between the gas and the liquid phase that occurs in the pores of the membrane; therefore, the morphology (i.e., the pore size and porosity of the membrane) is also important.

The impregnation of these ionic liquids onto a ceramic support involves physical or chemical interactions with the pore walls; hence, in the preparation of SILMs, the greater the membrane porosity, the better the performance [14–17]. Thus, three methods have been reported to support ionic liquids into the porous membranes: Direct immersion [17], pressurization [18], and vacuum [17–19].

Most reported work on supported ionic liquids membranes used organic polymeric supports. However, there are only a few reported that worked with ionic liquids supported over ceramics for such a purpose. In this paper, the aim was to select a simple ionic liquid (physical adsorption) and a tubular porous crystalline zirconia support, for studying the ILs stability once it were located in the support pores and the possible influence on permeation properties. The immersion method was selected to prepare two SILMs using two ILs [19]. Hence, the main aim of this work was to elucidate the strength of the chemical interaction between the ILs and the zirconia supports through IR spectroscopy studies, to understand whether or not any orientation of the ILs into the pore could influence the CO_2 separation. Additionally, the possible impacts on the permeability and separation factor for a CO_2/N_2 mixture using these SILMs, at different temperatures, was examined.

2. Materials and Methods

2.1. Materials Chemicals and Materials

CO_2 (99.998%, INFRA México, S.A. de C.V. Mexico City, Mexico) and nitrogen (99.99%, INFRA México, S.A. de C.V. Mexico City, Mexico) were used. Table 1 lists the ionic liquids used in this research. The ILs tested were 1-butyl-3-methyl imidazolium hexafluorophosphate ([C_4mim][PF_6]) and 1-butyl-3-methyl imidazolium tetrafluoroborate ([C_4mim][BF_4]). The molecular structures of the ionic liquids are shown in Figure 1. The physical properties of the ILs, such as density, melting point, viscosity and surface tension, are shown in Table 1 [20–22]. The ionic liquid, [C_4mim][PF_6], was purchased from Aldrich.

Table 1. Physical properties of the ionic liquids used in this study.

Ionic Liquid	Short Name	Molecular Weight ($g \cdot mol^{-1}$)	Density ($g \cdot mL^{-1}$) 20 °C	Melting Point (°C)	Viscosity (cP)	Surface Tension $mN \cdot m^{-1}$
1-butyl-3-methyl imidazolium tetrafluoroborate	[bmim][BF_4]	226.02	1.064	−71 °C	34	44.81
1-butyl-3-methyl imidazolium hexafluorophosphate	[bmim][PF_6]	284.18	1.38	12 °C	450	43.52

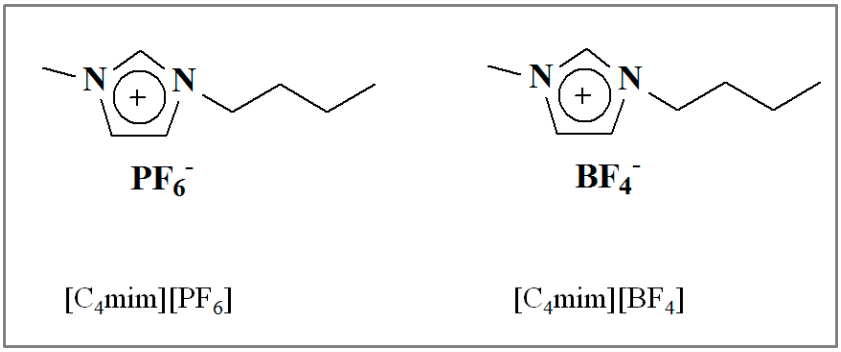

Figure 1. Molecular structures of the ionic liquids.

2.2. Synthesis of 1-Butyl-3-Methylimidazolium Tetrafluoroborate ([C_4mim][BF_4])

The synthesis of [C_4mim][BF_4] was carried out following the procedures of Dupont et al., using [C_4mim]Cl (white solid) as the feedstock [23]. 1-butyl-3-methylimidazolium tetrafluoroborate was synthesized as follows: 91.6 g (0.52 mol) of 1-butyl-3-methylimidazolium chloride was added to 200 mL distilled water with potassium tetrafluoroborate, and the reaction solution was stirred at room temperature (0.1 bar) at 80 °C for 24 h to obtain 1-butyl-3-methylimidazolium tetrafluoroborate as a light yellow, viscous liquid. The structure was confirmed by FTIR (Excalibur, Varian Inc., Palo Alto, CA, USA) and ^{1}H and ^{13}C-NMR spectroscopy (Avance DMX500, Bruker BioSpin AG, Fällanden, Switzerland). 1-butyl-3-methylimidazolium tetrafluoroborate: FTIR: 3183, 3121, 2969, 2939, 2888, 1582, 1471, 1157, 1015, 763 cm^{-1}. ^{1}H-NMR (300 MHz, DMSO, δ/ppm relative to TMS) δ: 0.92 (*t*, *3H*, $^3J_{HH}$ = 7.3), 1.27 (*m*, *2H*), 1.71 (*m*, *2H*), 3.84 (*s*, *3H*), 4.16 (*t*, *2H*, ^3J = 7.4, *1H*), 7.74 (*s*, *1H*) 7.67 (*s*, *1H*), 9.07 (*s*, *1H*) ppm. ^{13}C-NMR (75 MHz, DMSO) δ: 13.3, 18.8, 31.4, 35.7, 48.6, 122.3, 123.6, 136.6 ppm (Figures S1 and S2 in Supplementary Materials).

2.3. ZrO_2-Al_2O_3 Support

Commercial tubular membranes (15 cm length, 0.7 cm ID, 1 cm OD, and 2.5 cm glazed ends) were purchased from Pall Corporation (Figure 2a) and used as supports for the ionic liquids. The tubes comprised an inner mesoporous zirconium oxide layer (mean pore diameter of 0.02 μm and thickness of 4 μm) and two α-alumina layers with mean pore diameters of 0.2 μm and 0.9 μm and thicknesses of 20 and 40 μm, respectively (Figure 2b).

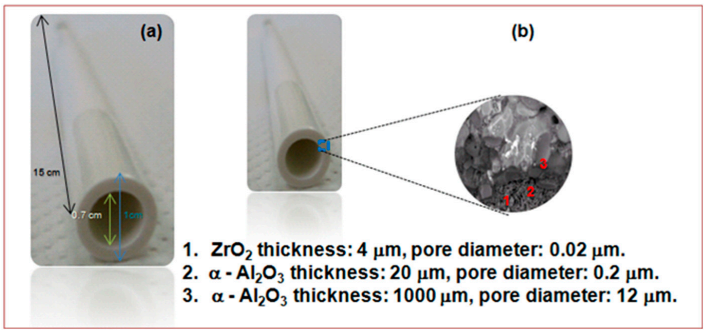

Figure 2. (**a**) Dimensions of the supported ionic liquid membranes (SILMs) and (**b**) cross-sectional image of the ZrO_2-Al_2O_3 support, indicating the average pore diameters and thicknesses of the various layers.

2.4. Preparation of Supported Ionic Liquid Membranes

Due to their high viscosities, the ILs were dissolved in ethanol (10 wt %). All SILMs used throughout this study were supported in the following manner. The ZrO_2-Al_2O_3 support was placed in a glove box under vacuum and was subsequently covered with Teflon® tape (Garlock 1/2 "X 260", Ciudad de México, Mexico) on the outside of the tubular support, and after impregnation the Teflon tape was removed. The pores of the inorganic support were impregnated with the ionic liquid-ethanol solution. Then, the excess ionic liquid-ethanol solution was removed by evaporation, leaving only the remaining non-volatile ionic liquid within the support pores. The amount of ionic liquid deposited was determined by weighing the membrane before and after ILs immobilization, and the thickness was estimated according to Equation (1):

$$\delta_{\mathrm{ILs}} = \frac{m_{ILs}}{A\rho_{ILs}} \quad (1)$$

where A, m, and ρ are membrane inner areas of the support, mass, and density, respectively. The subscript ILs means ionic liquid. The density data of the ILs used in this work are listed in Table 1.

2.5. Estimation of the Trans-Membrane Pressure

Several authors have used the Trans-membrane pressure to estimate the pressure necessary to displace the liquid supported into the mesopores under pressure [24,25]. The Young–Laplace Equation (2) was used to estimate this pressure, where P_{IL} is the capillary pressure of the ionic liquid, γ is the surface tension of the ionic liquid, θ is the contact angle and d is the pore diameter. Complete wetting of the support material b he Trans-membrane pressure, ΔP, necessary to balance the capillary forces of the liquid within the pores with the gas pressure.

$$\Delta P_i = \frac{4\gamma_{ILs}\cos\theta}{d} \quad (2)$$

The surface tension values of the ILs at 25 °C, shown in Table 1, were obtained from the literature. P_{IL} values were 89.6 and 87 bar for [C_4mim][BF_4] and [C_4mim][PF_6], respectively, in a layer of ZrO_2 support with a pore size of 0.02 μm. ΔP_i is the Trans-membrane driving force of component "*i*" that passes through the membrane.

2.6. Ionic Liquid and SILM Characterization

A scanning electron microscope (SEM) (ESEM XL-30, Philips, Eindhoven, The Netherlands) was used to study the topography, morphological appearance, and microstructure of the support and SILMs. Energy dispersive spectroscopy (EDS) analyses (XL50, EDAX, Philips, Eindhoven, The Netherlands) were used to determine the overall chemical composition of the membranes and the distribution of the chemical elements of interest in the SILMs. Fourier transform infrared (FTIR) measurements, carried out in the 350–4000 cm^{-1} wavenumber range, were performed with a Varian 3600 spectrometer (Varian Inc., Palo Alto, CA, USA) to obtain the spectra of the ZrO_2-Al_2O_3 support, [C_4mim][PF_6], [C_4mim][BF_4] and the SILMs, as well as to study the chemical groups on the support surface before and after ionic liquid impregnation. FTIR spectra were directly obtained using a diffuse reflectance (DR) accessory on the surfaces of the samples.

2.7. Evaluation of SILMs and Single Gas Permeances of CO_2 and N_2

Permeability experiments were conducted following the standard test method of ASTM D1434 using the volumetric procedure, *V*, in which the lower pressure chamber was maintained near atmospheric pressure, and the volumetric feed rate of the CO_2 and N_2 passing through the SILMs is indicated by the gas volume per unit time, V_r, measured in a flowmeter [26]. A schematic diagram of the experimental setup for obtaining CO_2 and N_2 permeances is shown in Figure 3. A couple of Viton joints were used for fitting the SILMs to the metal cylinder. The configuration for the permeation module was divided into two chambers. The core side was used for feeding the single gas, i.e., CO_2 or N_2, and the feed side compartment of the permeation module was connected to a pressure transducer (PT). The pressure at the feed side was in the 1–3 bar range for all measurements. A thermocouple was placed into the permeation module, and a heating tape surrounded the permeation module to maintain the temperature throughout the permeance test, which was measured by a thermocouple (TW) connected to a temperature indicator (TI). The gas permeation rates of the SILMs for CO_2 and N_2 gases were measured after a period of 210 min required for reaching a steady state.

Gas transport through the SILMs was assumed to follow a solution-diffusion mechanism. The permeability of species i (Pi) is based on kinetic transport (diffusivity, Di) and thermodynamic affinity (solubility, Si) in the membrane.

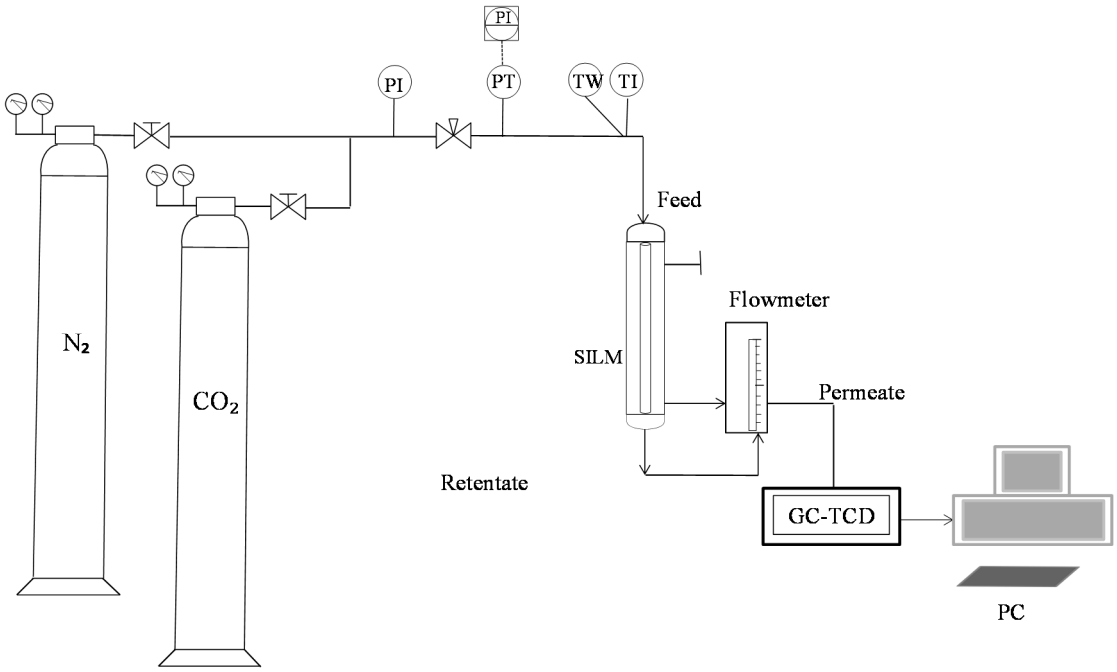

Figure 3. Experimental setup for measuring the permeability and separation factor of CO_2 and N_2 for a CO_2/N_2 mixture in the SILMs.

The flux (F) through the SILMs was calculated from Equation (3), where V_r is the volumetric feed rate, A is the transfer cross section, p_o is the ambient pressure, R is the universal gas constant, and T is the ambient temperature:

$$F = \frac{\left(10^{-6}\right)\left(p_o\right)\left(V_r\right)}{ART} \tag{3}$$

Therefore, the permeance, P, is defined as the ratio between the flux and the partial pressure differential across the barrier, and because the SI unit of pressure is the Pascal, appropriate SI units for the permeance are mol/m^2·s·Pa. The permeance was obtained as follows:

$$P = \frac{F}{p - p_o} \tag{4}$$

The ideal selectivity (α) is used as a measure of the separation efficiency, which is represented by the ratio between the permeances of CO_2 and N_2 as shown:

$$\alpha = \left(\frac{P_{CO_2}}{P_{N_2}}\right) \tag{5}$$

A schematic diagram of the experimental setup for the separation factor is shown in Figure 3. An equimolar CO_2/N_2 gas mixture was fed to the core side of the permeation module, and the effective membrane area was approximately 44 cm^2. The pressure at the feed side of the membrane module ranged from 1 to 3 bar, while the permeate side was at atmospheric pressure. The CO_2 and N_2 gas mixture at the permeate and retentate sides were analysed by gas chromatography (GC) coupled to a TCD detector, to determine the composition of the gases. For a separation test, the membrane was dried by purging with pure N_2 at 200 °C. No sweep gas was used in these experiments.

Koros et al. [27], suggested a terminology for membranes and membrane processes, where the separation factor (S_F) is defined in terms of the ratio of the mole fractions of CO_2 and N_2 gases in the permeate side relative to that in the retentate side, as shown:

$$S_F(CO_2/N_2) = \left[X_{CO_2}/X_{N_2}\right]_{permeate} / \left[X_{CO_2}/X_{N_2}\right]_{retentate} \quad (6)$$

3. Results and Discussion

3.1. SEM/EDX Characterization of the ZrO_2 Support

SEM analyses coupled with EDX permitted the study of the morphological appearance, porosity, layer stratification, and the overall chemical composition. The morphological study of the support (see Figure 4a) showed three layers with thicknesses of 4, 15, and 50 µm for ZrO_2 and alfa-Al_2O_3, respectively. The two outermost layers of the alfa-Al_2O_3 consisted of mesoporous and macroporous layers, and the thicknesses were estimated in reference to the scale appearing at the lower side of the micrograph in Figure 4a, validating the thicknesses reported in Figure 2. The EDX result shown in Figure 4b is an analysis of the ZrO_2-Al_2O_3 support, displaying the characteristic peaks assigned to the Kα lines of O, Al, and Zr. The relative elemental contents were 49.51%, 27.43%, and 23.06% for O, Zr, and Al, respectively.

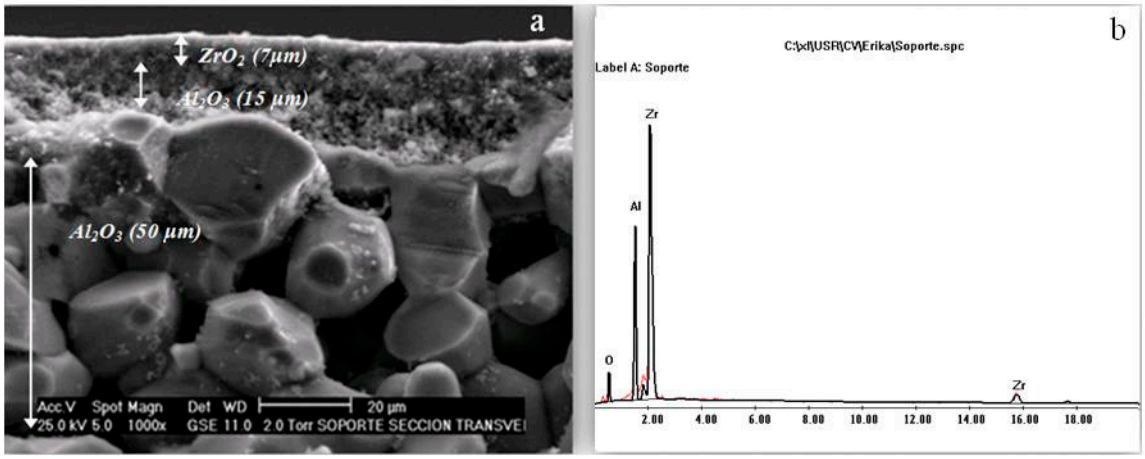

Figure 4. SEM secondary electron image of the (**a**) ZrO_2-Al_2O_3 support and (**b**) EDX spectra of ZrO_2-Al_2O_3.

3.2. Study of the Interaction of ILs with the ZrO_2 Support

After immobilization of the ILs ([C_4mim][PF_6] and [C_4mim][BF_4]) in the ZrO_2-Al_2O_3 support, the SILMs were analysed to confirm their loadings into the pores of the support and to verify their homogeneous distributions in the radial direction. The SEM micrographs of the membrane cross-section (Figure 5a) and the EDX spectrum (Figure 5c) correspond to the square area formed by the white line for the [C_4mim][PF_6] SILMs, which revealed the characteristic O, Al, Ca, F, P, Si, and Zr peaks with the following atomic percentages: 50.4, 37.4, 3.5, 4.3, 2.2, 1.2, and 0.96 at.%, respectively. Furthermore, the chemical composition data confirmed the presence of the ionic liquid in the ZrO_2 layer and in the intermediary mesoporous alfa-Al_2O_3 film.

Similar results were obtained for the [C_4mim][BF_4] SILMs, which revealed the O, Al, Ca, F, Si, and Zr peaks with the following atomic percentages: 56.9, 23.5, 3.6, 13.8,1.3, and 0.9 at.%, respectively. It can be preliminarily concluded that most of the ionic liquid was deposited on the internal support surface (ZrO_2), and the intermediate macropores of the alfa-Al_2O_3 were partially filled. Therefore, it was possible to estimate the thicknesses of the [C_4mim][PF_6] and [C_4mim][BF_4] SILMs, as shown Table 2. All of the elements identified are part of the chemical composition of each SILM. Therefore, in view of these observations, the SEM-EDX techniques indicate that different amounts of ILs were immobilized in the internal layers of the support with a relatively homogeneous distribution.

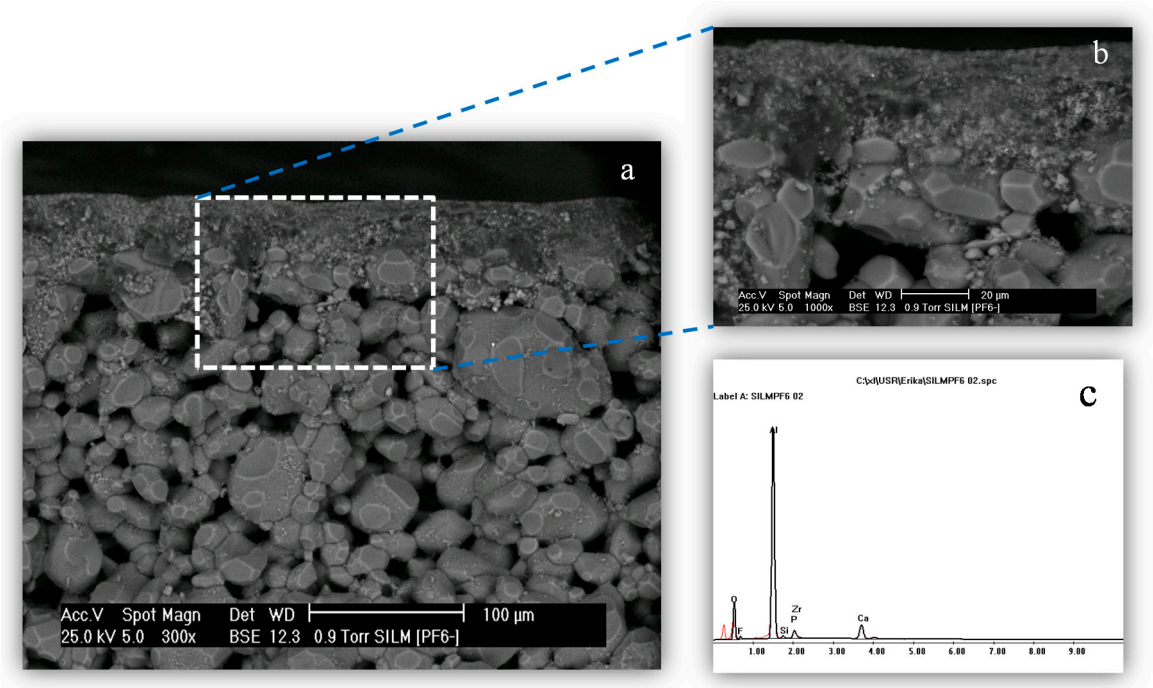

Figure 5. Scanning electron micrographs of the (**a**) [C_4mim][PF_6] SILMs; (**b**) magnification (1000×) of the membrane; and (**c**) EDX spectra of the [C_4mim][PF_6] SILMs.

Table 2. The results of elemental chemical analysis of SILMs.

SILM	Thickness (µm) Estimated through Equation (1)	Thickness (µm) Estimated by SEM
[bmim][BF_4]	25.64	25
[bmim][PF_6]	72.02	65

The thicknesses of the ionic liquids over the ZrO-Al_2O_3 supports calculated by Equation (1), and those estimated by scanning electron microscopy are shown in Table 2. The thickness of the [C_4mim][PF_6] SILMs is larger than that of the [C_4mim][BF_4] SILMs.

This difference in the thicknesses can be attributed to the fact that [C_4mim][PF_6] is more viscous than [C_4mim][BF_4] (Table 1) and, consequently, exhibits the highest IL retention in the porous support.

3.3. FTIR (DR)

The interaction of ILs with the support was studied by FTIR. Figure 6a shows the IR spectrum for a layer of the ZrO_2 support (red line). The surface spectrum shows that OH^- stretching bands are located in the 3000 to 3780 cm^{-1} region, and at 1615 cm^{-1}, the intensity of the OH^- groups of the top support layer shows that charges are present at the surface. In the spectra of ILs [C_4mim][BF_4] (blue line) and SILMs ([C_4mim][BF_4]) (black line), both display the CH stretching modes and the characteristic band of the imidazolium ring. In particular, Figure 6a shows that in the 2800–3400 cm^{-1} regions, it is possible to identify bands corresponding to the CH_2 and CH_3 stretching vibrations of the alkyl groups at the nitrogen atoms of the imidazolium ring. The peaks at 3125 and 3164 cm^{-1} are assigned to the symmetric and antisymmetric stretching modes of HC(4)-C(5)H, denoted as ν_aHC(4)C(5)H and ν_sHC(4)C(5)H, respectively, and the shoulder seen at approximately 3114 cm^{-1} for C(2)-H is denoted as νC(2)H. The band at approximately 1570 cm^{-1} is due to the ring stretching vibration of the imidazole group. The assignments were made in accordance with the literature for anions and cations [28–30]. Moreover, the ZrO_2-Al_2O_3 support does not show bands in the 3200–2000 cm^{-1} range; however, it exhibits absorption in the 1700–800 cm^{-1} range.

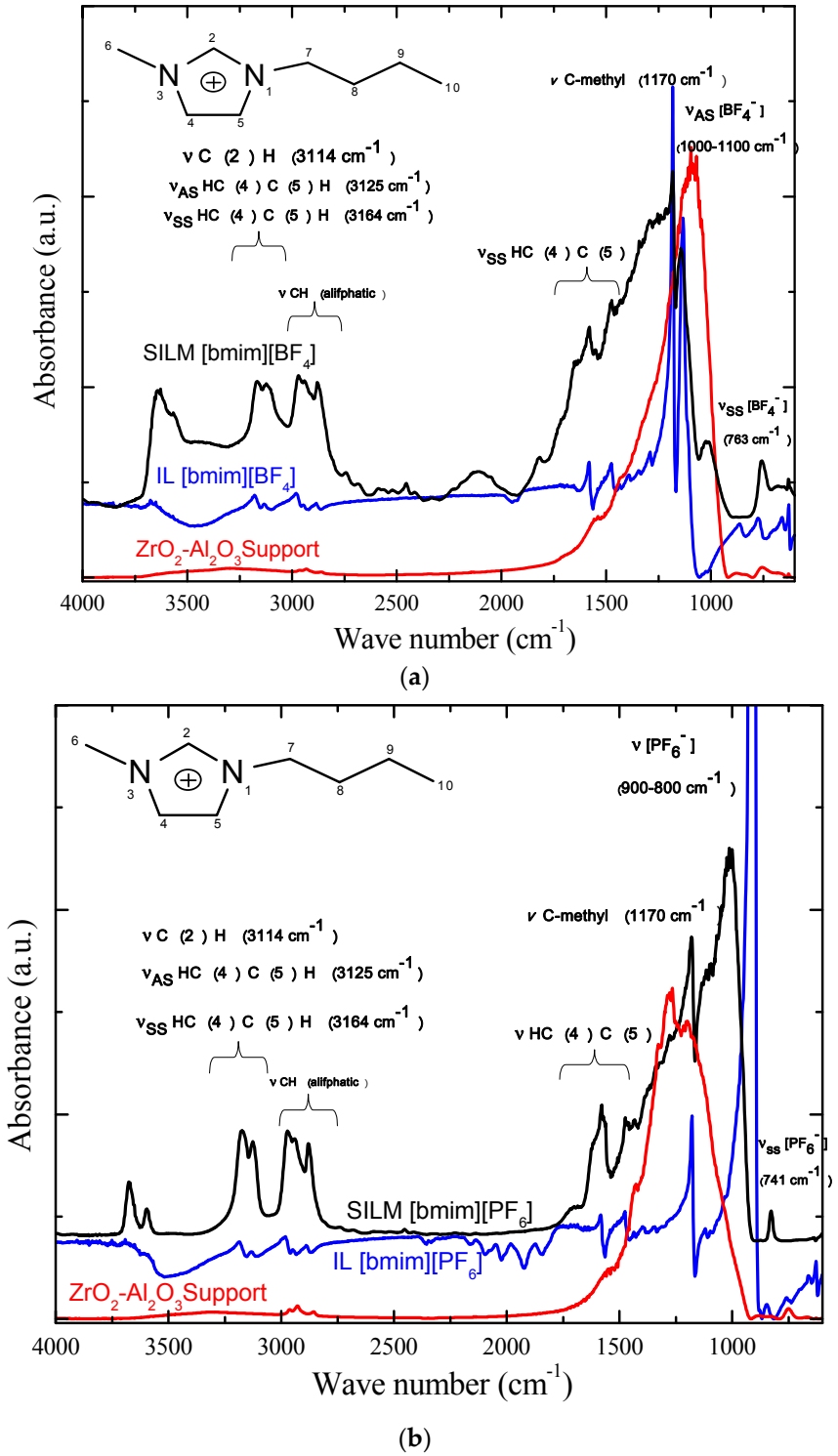

Figure 6. FTIR spectra recorded between 4000 and 600 cm^{-1} showing (**a**) comparison of the ZrO_2 support, the $[C_4mim][BF_4]$ IL, and the $[C_4mim][BF_4]$ SILMs and (**b**) comparison of the ZrO_2 support, the $[C_4mim][PF_6]$ IL, and the $[C_4mim][PF_6]$ SILMs.

After permeation testing, the membrane was cut, FTIR analysis was carried out on the inner surface of the membrane tube, and the analysis presented refers to the inside of the membrane. The infrared spectra of the two supported and unsupported ionic liquids show minimum changes in the bands assigned to their anions. However, the greatest intensity change occurred in the absorption

bands corresponding to the cations of the ionic liquids, particularly for the carbon assigned to the proton at position two of the imidazole ring, i.e., C(2)-H, suggesting that this interaction is between the ionic liquids and the ZrO_2 support. This provides evidence that the IL interacts at the molecular level with the porous wall and also allows the ILs to accommodate adequately within the pores through a dipole interaction between the ILs and the porous wall. As a result, the imidazolium cation in the pores is oriented perpendicularly to the surface of the membrane. Furthermore, the cation will be oriented toward the outer surface, while the anion will be toward the bulk of the liquid. This behaviour has been predicted by a diverse number of studies, including neutron reflectometry (NR), X-ray reflectivity (XR or XRR), and molecular dynamics (MD) simulation, which showed that the density at the surface is greater than that at the bulk. Using the rules reported by Lovelock [31], however, when the ionic liquid is supported, we observed intensity changes in the bands, thereby suggesting changes in the orientation due to the aforementioned interaction. This was shown before and after the impregnation of the ionic liquid, as depicted in Figure 6. Based on this analysis, it can be suggested that the IR spectra provided a first indication of the interaction and orientation of the cation within the ZrO_2 support. In fact, these results strongly suggest an orientation of the ionic liquid with the imidazolium cation due to the interaction with the ZrO_2-Al_2O_3 support. These effects bring in an associated change in the thermodynamics of the ILs confined to the bulk fluid and, consequently, it can modify the solubility of the gas in the ionic liquid; this is due to a liquid confinement effect in the mesoporous support. Figure 6 also shows the spectral region where the anion bands predominate. With respect to the anion-related intensity bands between 1200 and 1400 cm^{-1}, the assignment of the various spectral groups were due to the antisymmetric stretching modes (νSO_2IR); the spectrum of the ILs shows that the [C_4mim]-related absorption band originates from the ring stretching at approximately 1570 cm^{-1}. Additionally, it can be seen that the [C_4mim]-related spectral features are less pronounced for the unsupported ionic liquid than for the supported ionic liquid. Similar behaviours were found for the [C_4mim][PF_6] ionic liquid, as shown in Figure 6b. This result confirms that the main interaction is between the cation and the inner surface of the pores of the support.

3.4. CO_2 Separation Performance

Figure 7a,b present the CO_2 and N_2 single gas permeances vs. the Trans-membrane pressure for the [C_4mim][BF_4] and [C_4mim][PF_6] SILMs, respectively. The CO_2 permeance through the [C_4mim][BF_4] SILMs was large, i.e., 9.6×10^{-7} $mol \cdot s^{-1} \cdot m^{-2} \cdot Pa^{-1}$, whereas that of N_2 was 8.8×10^{-8} $mol \cdot s^{-1} \cdot m^{-2} \cdot Pa^{-1}$. Furthermore, a similar behaviour was observed in the [C_4mim][PF_6] SILMs, i.e., 1.4×10^{-7} $mol \cdot s^{-1} \cdot m^{-2} \cdot Pa^{-1}$ for CO_2 and 1.88×10^{-8} $mol \cdot s^{-1} \cdot m^{-2} \cdot Pa^{-1}$ for N_2. Hence, the CO_2 permeability was 10 times and seven times greater than that of N_2 in [C_4mim][BF_4] and [C_4mim][PF_6], respectively. We disregarded the facilitated transport occurring in the SILMs due to humidity because we were particularly careful in drying the ionic liquid. In all of the permeance tests, the SILMs were tested at increasing and decreasing pressures repeatedly to verify that the ionic layer remained intact within the pore network of the support, until the pressure reached 3 bar; the results showed that the SILMs remained stable after the permeability tests. The solution-diffusion model was used to describe the permeation process. The results clearly indicate that the permeance decreased with the increase of CO_2 pressure, although at 2 bar, the permeance slowly decreased with further pressure increase. A simplified model of the ideal gas permeance can be expressed in terms of the solubility coefficient and the diffusion coefficient when the ILs is saturated with CO_2. It turns out that the permeation was quasi-constant with a pressure increase. This behaviour can be explained by the transport mechanism through the ionic liquid, which is described by solution-diffusion mass transport processes when the maximum driving force is directly related to the CO_2 solubility in the ionic liquid [32–40]. The N_2 permeance through the [C_4mim][BF_4] and [C_4mim][PF_6] SILMs remained below the CO_2 permeance with the increase in the Trans-membrane pressure.

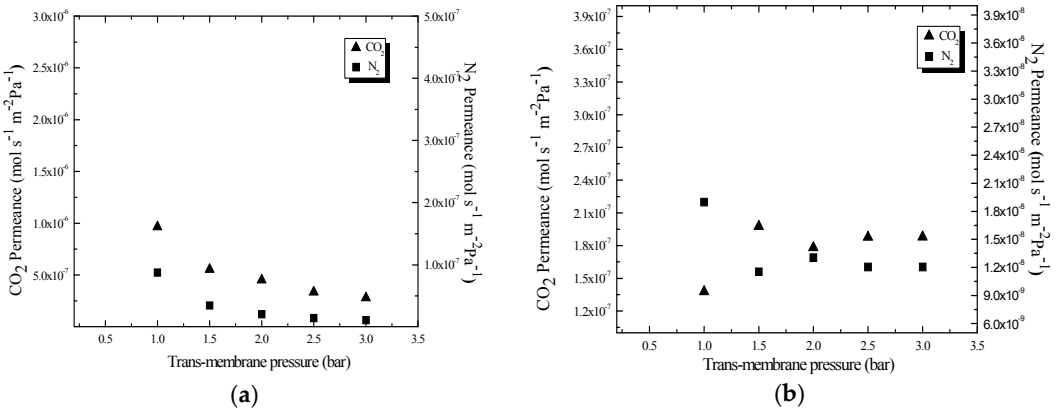

Figure 7. CO_2 and N_2 permeances as a function of the trans-membrane pressure at 25 °C in (**a**) [C_4mim][BF_4] and (**b**) [C_4mim][PF_6].

3.5. Effects of ILs Anion Species on Permeance

The effects of the two different anions on permeance are shown in Figure 7a,b. The comparison of SILMs bearing different anions reveals that the degree of interaction of the anions with CO_2 decreased in strength from the highest to the lowest CO_2 permeance. The best performance was for the [C_4mim][BF_4] SILMs displaying the largest CO_2 permeability. A possible explanation for this considers the acid-base interactions between the CO_2 and the ionic liquids, in that the [BF_4] anion behaves as a stronger Lewis base than the [PF_6] anion, i.e., the [BF_4] anion forms a stronger interaction with CO_2 in acting as a base to this molecule. Kazarian and co-workers showed evidence of chemical interactions between the anion and the CO_2, which supports our suggestion above, although they stated that those interactions were probably not large enough to be the sole factor leading to the high CO_2 solubility [28]. They observed Lewis acid-base interactions where the anion acts as a Lewis base. Molecular simulations of CO_2 in [C_4mim][PF_6] also showed CO_2 molecules located around the anions [41].

3.6. Effects of Temperature on the Permeance in SILMs

Figure 8 shows the general trend of the permeance of CO_2 for five different temperatures. Here, the permeance decreased as the temperature increased in the entire pressure range, and this trend can be explained by the decrease of CO_2 solubility as the temperature increases [42]. An important change takes place between 80 and 120 °C, in which CO_2 due to increased temperature. Moreover, the CO_2 solubility is enhanced with increasing pressure at constant temperature but does not compensate for the decreased solubility with increasing temperature. As a preliminary conclusion, the SILMs remained stable throughout the permeance tests with varying temperature and pressure.

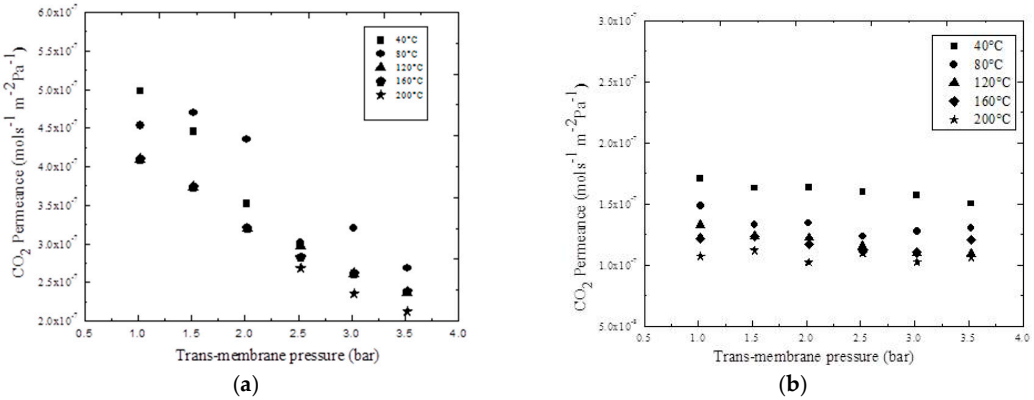

Figure 8. CO_2 permeance in SILMs at different temperatures: (**a**) [C_4mim][BF_4] and (**b**) [C_4mim][PF_6].

3.7. CO_2/N_2 Ideal Selectivity for Different SILMs

Figure 9a shows the single gas CO_2/N_2 ideal selectivity in different SILMs as a function of the trans-membrane pressure. The CO_2/N_2 ideal selectivity slightly increased from 1 to 2 bar for $[C_4mim][BF_4]$ and $[C_4mim][PF_6]$. This behaviour may be associated with the increase of CO_2 solubility when the gas pressure is increased for the ILs [36–43], resulting in a higher affinity for CO_2 than N_2. When the pressure increased from 2 to 3 bar, the CO_2/N_2 ideal selectivity increased very slightly, which means that the solubility is close to the saturation of ILs by both gases. This causes the ideal selectivity to remain quasi-constant in agreement with the report by Lozano et al., because ideal selectivity depends mainly on the nature of the ILs used as the liquid phase [35]. The relatively high ideal selectivity, i.e., α (CO_2/N_2) = 25, for the $[C_4mim][BF_4]$ IL on ZrO_2-Al_2O_3 may suggest the use of $[C_4mim][BF_4]$ SILM as an alternative material for CO_2/N_2 separation at temperatures from ambient temperature to 120 °C, in which the IL remains stable with a high solubility for CO_2.

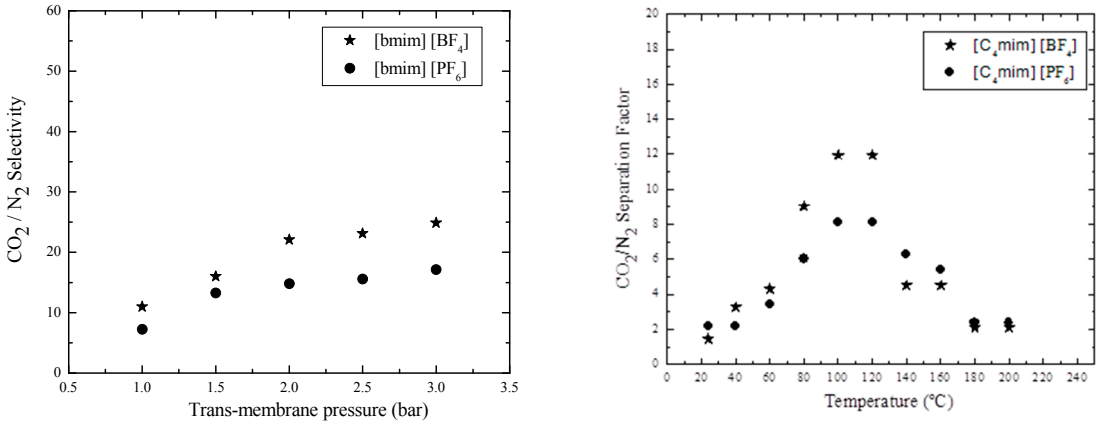

Figure 9. (**a**) CO_2/N_2 selectivity for $[C_4mim][BF_4]$ and $[C_4mim][PF_6]$ SILMs as a function of the trans-membrane pressure at 25 °C and (**b**) separation factor of mixed CO_2/N_2 for $[C_4mim][PF_4]$ and $[C_4mim][PF_6]$ SILMs as a function of temperature.

3.8. Separation Factor

The effect of temperature on the separation factor of the mixed CO_2/N_2 is shown in Figure 9b. It is interesting to note that the trend displayed a maximum at 80–100 °C, which is observed in both SILMs, and with increasing temperature, the separation factor decreases slightly. In fact, when the temperature increases, the CO_2 solubility decreases, and its diffusion in the ILs film increases. This suggests that when the temperature increases in the 20–100 °C range, CO_2 diffusion is active in the ILs film despite the decrease in solubility at the gas phase-ionic liquid interface. However, at temperatures exceeding 100 °C, the increased diffusion cannot compensate for the decrease in solubility, resulting in a slight decrement of the separation factor. On the basis of the ideal selectivity and separation factor, the results obtained shown in Figure 9, the membrane ideal selectivity for a single gas is larger than the separation factor for mixed gases. In the latter case, the driving force is generated by applying a pressure difference across the membrane, and it is possible that there is a competition between CO_2 and N_2 gases through the SILMs.

3.9. Loss of Ionic Liquids after CO_2 Separation

Figure 10 shows the weight loss of ILs in the SILMs at different temperatures at 2 bar of pressure. Therefore, this result shows that under the working conditions, there is negligible evaporation of the liquid and that there is no displacement of liquid out of the pores, so the SILMs present good stability.

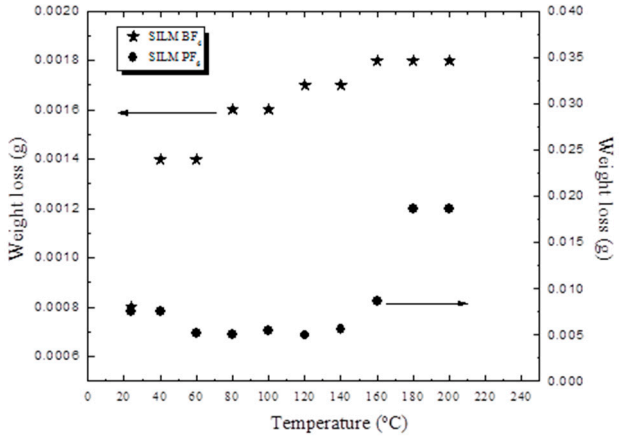

Figure 10. SILMs weight loss of ILs after CO_2 separation.

4. Conclusions

The FTIR and SEM results showed that the ionic liquid had been adequately immobilized in the porous network support. Under particular conditions of the FTIR experiment, the IR intensity change in the absorption bands demonstrated the interaction between the ILs cation and the surface of the support, which exhibits a negative charge due to the hydroxyl group of the support; therefore, this results showed an important interaction between the ILs and the support which causes an orientation effect of the molecule of the ILs confined into the pores. The ILs immobilization method allowed a good loading, as well as contributed to the stability of IL in the pores under pressure, which is an important element in the permeability performances of the SILMs. The separation of CO_2 from N_2 was successfully carried out with ILs supported on ceramic supports. In agreement with permeability studies, it was found that the anions dominated the interactions with CO_2; experimentally, it was found that the BF_4 anion had a greater affinity for CO_2 when compared with the PF_6 anion. The separation factor value in the 80 to 120 °C range suggested that the membrane can be applied in a CO_2 separation process. The liquid loss in the SILMs membranes after the permeability studies is closely related to support–ionic liquid interactions. Therefore, the SILMs are a very promising technology for CO_2 separation that can be used in a post-combustion system.

Supplementary Materials: The following are available online at www.mdpi.com/2227-7080/4/4/32/s1, Figure S1: ^{1}H NMR spectrum at 300 MHz of the ionic liquid [C4mim][BF4], Figure S2: ^{13}C-NMR spectrum at 300 MHz of the ionic liquid [C4mim][BF4].

Acknowledgments: We gratefully acknowledge financial support from CONACyT (Grant No. 56770 and 166208). VMA, MGA and TRM thank the SNI for the distinction of their membership and the stipend received.

Author Contributions: Mirella Gutierrez-Arzaluz, Violeta Mugica-Álvarez, Miguel Torres-Rodríguez and Cinthia E. Sánchez-Fuentes performed the experiments, conceived and designed the experiments and wrote the paper, Eduardo Terrés was in charge of the SEMs analysis, Sibele B. Pergher did the Synthesis of the ionic liquid and analyzed the data.

Conflicts of Interest: The authors declare no conflicts of interest.

References

1. Zhao, W.; He, G.; Nie, F.; Zhang, L.; Feng, H.; Liu, H. Membrane liquid loss mechanism of supported ionic liquid membrane for gas separation. *J. Membr. Sci.* **2013**, *411*, 73–80. [CrossRef]
2. Zhao, L.; Riensche, E.; Menzer, R.; Blum, L.; Stolten, D. A parametric study of CO_2/N_2 gas separation membrane processes for post-combustion capture. *J. Membr. Sci.* **2008**, *325*, 284–294. [CrossRef]
3. Department of the New Energy and Industrial Technology Development Organization (NEDO). Ceramic membrane to combat global warming. *Membr. Technol.* **1997**, *92*, 11–12.

4. Albo, J.; Yoshioka, T.; Tsuru, T. Porous Al_2O_3/TiO_2 tubes in combination with 1-ethyl-3-methylimidazolium acetate ionic liquid for CO_2/N_2 separation. *Sep. Purif. Technol.* **2014**, *122*, 440–448. [CrossRef]
5. Kumar, R.V.; Ghoshal, A.K.; Pugazhenthi, G. Fabrication of zirconia composite membrane by in-situ hydrothermal technique and its application in separation of methyl orange. *Ecotoxicol. Environ. Saf.* **2015**, *121*, 73–79. [CrossRef] [PubMed]
6. Tome, L.C.; Marrucho, I.M. Ionic liquid-based materials: A platform to design engineered CO_2 separation membranes. *Chem. Soc. Rev.* **2016**, *45*, 2785–2824. [CrossRef] [PubMed]
7. Dai, Z.; Noble, R.D.; Gin, D.L.; Zhang, X.P.; Deng, L. Combination of ionic liquids with membrane technology: A new approach for CO_2 separation. *J. Membr. Sci.* **2016**, *497*, 1–20. [CrossRef]
8. Rodríguez-Pérez, L.; Coppel, Y.; Favier, I.; Teuma, E.; Serp, P. Imidazolium-based ionic liquids immobilized on solid supports: Effect on the structure and thermostability. *Dalton Trans.* **2010**, *39*, 7565–7568. [CrossRef] [PubMed]
9. Blath, J.; Christ, M.; Deubler, N.; Hirth, T.; Schiestel, T. Gas solubilities in room temperature ionic liquids—Correlation between RTiL-molar mass and Henry's law constant. *Chem. Eng. J.* **2011**, *172*, 167–176. [CrossRef]
10. Kanakubo, M.; Aizawa, T.; Nanjo, H.; Kameda, Y.; Amo, Y.; Usuki, T. Liquid structures of 1-butyl-3-methylimidazolium tetrafluoroborate and carbon dioxide mixtures by X-ray diffraction measurements. *Fluid Phase Equilibria* **2010**, *297*, 183–186. [CrossRef]
11. Kerlé, D.; Ludwig, R.; Geiger, A.; Paschek, D. Temperature dependence of the solubility of carbon dioxide in imidazolium-based ionic liquids. *J. Phys. Chem. B* **2009**, *113*, 12727–12735. [CrossRef] [PubMed]
12. Anthony, J.L.; Brennecke, J.F. Solubilities and thermodynamic properties of gases in the ionic liquid 1-*n*-butyl-3-methylimidazolium hexafluorophosphate. *J. Phys. Chem. B* **2002**, *106*, 7315–7320. [CrossRef]
13. Anthony, J.L.; Anderson, J.L.; Maginn, E.J.; Brennecke, J.F. Anion effects on gas solubility in ionic liquids. *J. Phys. Chem. B* **2005**, *109*, 6366–6374. [CrossRef] [PubMed]
14. Carlisle, T.K.; Bara, J.E.; Gabriel, C.; Noble, R.D.; Gin, D.L. Interpretation of CO_2 solubility and selectivity in nitrile-funcionalized room-temperature ionic liquids using a group contribution approach. *Ind. Eng. Chem. Res.* **2008**, *47*, 7005–7012. [CrossRef]
15. Ruth, E.; Baltus, R.M.; Benjamin, H.; Culbertson, H.L.; David, W.; DePaoli, S.D.; Douglas, C. Examination of the potential of ionic liquids for gas separations. *Sep. Sci. Technol.* **2005**, *40*, 525–541.
16. Scovazzo, P.; Kieft, J.; Finan, D.A.; Koval, C.; Noble, R. Gas separations using non-hexafluorophosphate $[PF_6]^-$ anion supported ionic liquid membranes. *J. Membr. Sci.* **2004**, *238*, 57–63. [CrossRef]
17. Hernández, F.J.; De los Ríos, A.P.; Tomás, F.; Palacios, J.M.; Víllora, G. Preparation of supported ionic liquid membranes: Influence of the ionic liquid immobilization method on their operational stability. *J. Membr. Sci.* **2009**, *341*, 172–177. [CrossRef]
18. Fortunato, R.; González, M.J.; Kubasiewicz, M.; Luque, S.; Alvarez, J.R.; Alfonso, C.A.M.; Coelhoso, I.M.; Crespo, J.G. Liquid membranes using ionic liquids: The influence of water on solute transport. *J. Membr. Sci.* **2005**, *249*, 153–162. [CrossRef]
19. Malik, M.A.; Hashim, M.A.; Nabi, F. Ionic liquids in supported liquid membrane technology. *Chem. Eng. J.* **2011**, *171*, 242–254. [CrossRef]
20. Gardas, R.L.; Coutinho, A.P. Applying a QSPR correlation to the prediction of surface tensions of ionic liquids. *Fluid Phase Equilibria* **2008**, *265*, 57–65. [CrossRef]
21. Freire, M.G.; Carvalho, P.J.; Fernandes, A.M.; Marrucho, I.M.; Queimada, A.J.; Coutinho, J.A.P. Surface tensions of imidazolium based ionic liquids: Anion, cation, temperature and water effect. *J. Colloid Interface Sci.* **2007**, *314*, 621–630. [CrossRef] [PubMed]
22. Yu, G.; Zhao, D.; Wen, L.; Yang, S.; Chen, X. Viscosity of ionic liquids: Database, observation, and quantitative structure-property relationship analysis. *AIChE J.* **2011**, *58*, 2885–2899. [CrossRef]
23. Dupont, J.; Consorti, C.S.; Suárez, P.A.Z.; Souza, R. Preparation of 1-butyl-3-methyl imidazolium-based room temperature ionic liquids. *Org. Synth.* **2004**, *10*, 184.
24. Aki, S.N.; Mellein, B.R.; Saurer, E.M.; Brennecke, J.F. High-pressure phase behavior of carbon dioxide with imidazolium-based ionic liquids. *J. Phys. Chem. B* **2004**, *108*, 20355–20365. [CrossRef]
25. Kreiter, R.; Overbeek, J.P.; Correia, L.A.; Vente, F.J. Pressure resistance of thin ionic liquid membranes using tailored ceramic supports. *J. Membr. Sci.* **2011**, *370*, 175–178. [CrossRef]

26. Standard Test Method for Determining Gas Permeability Characteristics of Plastic Film and Sheeting. Available online: http://www.astm.org/Standards/D1434 (accessed on 5 August 2015).
27. Koros, W.J.; Ma, Y.H.; Shimidzut, T. Terminology for membrane and membrane processes. *J. Membr. Sci.* **1996**, *120*, 149–159.
28. Kazarian, S.G.; Briscoe, B.J.; Welton, T. Combining ionic liquids and supercritical fluids: In situ ATR-IR study of CO_2 dissolved in two ionic liquids at high pressures. *Chem. Commun.* **2000**, 2047–2048. [CrossRef]
29. Baiker, A.; Jutz, F.; Andanson, J.M. Investigation of binary and ternary systems of ionic liquids with water and/or supercritical CO_2 by in situ attenuated total reflection infrared spectroscopy. *J. Phys. Chem. B* **2010**, *114*, 2111–2117.
30. Jeon, Y.; Sung, J.; Seo, C.; Lim, H.; Cheong, H.; Kang, M.; Moon, B.; Ouchi, Y.; Kim, D. Structures of ionic liquids with different anions studied by infrared vibration spectroscopy. *J. Phys. Chem. B* **2008**, *112*, 4735–4740. [CrossRef] [PubMed]
31. Lovelock, R.J. Influence of the ionic liquid/gas surface on ionic liquid chemistry. *Phys. Chem. Chem. Phys.* **2012**, *14*, 5071–5089. [CrossRef] [PubMed]
32. Barghi, S.H.; Adibi, M.; Rashtchian, D. An experimental study on permeability, diffusivity, and selectivity of CO_2 and CH_4 through [bmim][PF_6] ionic liquid supported on an alumina membrane: Investigation of temperature fluctuations effects. *J. Membr. Sci.* **2010**, *362*, 346–352. [CrossRef]
33. Ramasubramanian, K.; Zhao, Y.; Ho, W.S. CO_2 Capture and H_2 purification: Prospects for CO_2-selective membrane processes. *AIChE J.* **2013**, *59*, 1033–1045. [CrossRef]
34. Kim, D.; Baek, H.; Hong, S.; Lee, H. Study on inmobilized liquid membrane using ionic liquid and PVDF hollow fiber as a support for CO_2/N_2 separation. *J. Membr. Sci.* **2011**, *372*, 346–354. [CrossRef]
35. Lozano, L.J.; Godínez, C.; Ríos, A.P.; Hernándes, F.J.; Segado, S.S.; Alguacil, F.J. Recent advances in supported ionic liquid membrane technology. *J. Membr. Sci.* **2011**, *376*, 1–14. [CrossRef]
36. Iarikov, D.D.; Hacarlioglu, P.; Oyama, S.T. Supported room temperature ionic liquid membranes for CO_2/CH_4 separation. *Chem. Eng. J.* **2011**, *166*, 401–406. [CrossRef]
37. Jian, Y.Y.; Zhou, Z.; Jiao, Z.; Li, L.; Wu, Y.T.; Zhang, Z.B. SO_2 gas separation using supported ionic liquid membranes. *J. Phys. Chem. B* **2007**, *111*, 5058–5061. [CrossRef] [PubMed]
38. Jiang, Y.; Wu, Y.; Wang, W.; Li, L.; Zhou, Z.; Zhang, Z. Permeability and selectivity of sulfur dioxide and carbon dioxide in supported ionic liquid Membranes. *Sep. Sci. Technol.* **2009**, *17*, 596–601. [CrossRef]
39. Larachi, F.; Siaj, M.; Rahman, M.H. Ionic liquids for CO_2 capture-development and progress. *Chem. Eng. Process. Process Intensif.* **2010**, *49*, 313–322.
40. Luis, P.; Neves, L.A.; Afonso, C.A.M.; Coelhoso, I.M.; Crespo, J.G.; Garea, A.; Irabien, A. Facilitated transport of CO_2 and SO_2 through supported ionic liquid membranes (SILMs). *Desalination* **2009**, *245*, 485–493. [CrossRef]
41. Cadena, C.; Anthony, J.L.; Shah, J.K.; Morrow, T.I.; Brennecke, J.F.; Marginn, E.J. Why is CO_2 so soluble in imidazolium-based ionic liquids. *J. Am. Chem. Soc.* **2004**, *126*, 5300–5308. [CrossRef] [PubMed]
42. Jindaratsamee, P.; Shimoyama, Y.; Morizaki, H.; Ito, A. Effects of temperature and anion species on CO_2 permeability and CO_2/N_2 separation coefficient through ionic liquid membranes. *J. Chem. Thermodyn.* **2011**, *43*, 311–314. [CrossRef]
43. Joan, F.; Brennecke, E.J. Ionic liquids: Innovative fluids for chemical processing. *AIChE J.* **2001**, *47*, 2384–2389.